Treatment Wastewater of Oil Refinery by Fe2O3 NPs produce by the novel Alishewanella Jeotgali strain HAQ8.

Hawraa Qays Al-assdy

Wijdan Hussein Al-Tamimi

Asia Fadhile Almansoory

University of Kerbala

Treatment Wastewater of Oil Refinery by Fe2O3 NPs produce by the novel Alishewanella Jeotgali strain HAQ8.

Abstract

Metal oxide nanoparticles like iron oxide (Fe_2O_3) exhibit strong reactivity and photolytic features in wastewater treatment and serve as an effective adsorbent for water purification due to its substantial surface area and affinity for different functionalized groups. Iron oxide nanoparticles) IONPs) are currently applied to treat oil-contaminated water. Fe_2O_3NPs were produced using an extracellular approach utilizing the *Alishewanella jeotgali* strain HAQ8. IONPs were characterized using UV-vis, FT-IR, XRD, AFM, SEM-EDX, and Zeta potential. λ max for the synthesized nanoparticles observed at (358) nm. The bands at 485 cm^{-1} in the FT-IR spectrum confirmed the formation of IONPs. The XRD showed that the IONPs' average crystallite size was (19) nm. According to AFM and SEM analyses, the surface roughness, maximum height, and mean diameter of Fe_2O_3NPs were (4.86, 18.36, and 48.8) nm, respectively, with spherical shapes. The Zeta potential of Fe_2O_3 NPs was (-43) mV. At 0.2 mg/mL Fe_2O_3 NPs, crude oil degradation reached (69.08) %, increasing to (71.4)% at pH 9. Fe_2O_3 NPs' cytotoxicity results indicated they were biocompatible with red blood cells even at the highest concentration. Fe_2O_3NPs produced by bacteria are harmless and non-toxic. Fe_2O_3NPs are expected to be potential candidates for crude oil degradation.

Keywords

Creative Commons License

RESEARCH PAPER

Treatment Wastewater of Oil Refinery by Fe₂O₃ NPs Produce by the Novel *Alishewanella jeotgali* Strain HAQ8

Hawraa Q. Al-assdy [a], Wijdan H. Al-Tamimi [a], Asia F. Almansoory [b,*]

[a] Department of Biology College of Science, University of Basrah, Iraq
[b] Department of Ecology, College of Science, University of Basrah, Iraq

Abstract

Metal oxide nanoparticles like iron oxide (Fe₂O₃) exhibit strong reactivity and photolytic features in wastewater treatment and serve as an effective adsorbent for water purification due to its substantial surface area and affinity for different functionalized groups. Iron oxide nanoparticles) IONPs) are currently applied to treat oil-contaminated water. Fe₂O₃NPs were produced using an extracellular approach utilizing the *Alishewanella jeotgali* strain HAQ8. IONPs were characterized using UV-vis, FT-IR, XRD, AFM, SEM-EDX, and Zeta potential. λ max for the synthesized nanoparticles observed at (358) nm. The bands at 485 cm^{-1} in the FT-IR spectrum confirmed the formation of IONPs. The XRD showed that the IONPs' average crystallite size was (19) nm. According to AFM and SEM analyses, the surface roughness, maximum height, and mean diameter of Fe₂O₃NPs were (4.86, 18.36, and 48.8) nm, respectively, with spherical shapes. The Zeta potential of Fe₂O₃ NPs was (−43) mV. At 0.2 mg/mL Fe₂O₃ NPs, crude oil degradation reached (69.08) %, increasing to (71.4) % at pH 9. Fe₂O₃ NPs' cytotoxicity results indicated they were biocompatible with red blood cells even at the highest concentration. Fe₂O₃NPs produced by bacteria are harmless and non-toxic. Fe₂O₃NPs are expected to be potential candidates for crude oil degradation.

Keywords: *Alishewanella jeotgali*, Fe₂O₃NPs, Biosynthesis, Treatment wastewater, Crude oil

1. Introduction

Water is essential to humans. With the advancement of humanity and the continuous consumption of water for industrial activities, the scarcity of freshwater resources has emerged as the most pressing issue that humanity must address immediately [1]. Akhter *et al.* [2] stated that the utilization of water resources has escalated with the growth of the global population and advancements in the industrial and agricultural sectors, resulting in increased water pollution with various contaminants. Toxic waste poses a serious threat to the well-being of both aquatic and terrestrial ecosystems [3]. Petroleum refineries are complex systems that involve multiple processes. The characteristics of refinery wastewater vary depending on the types of

crude oil processed, the intended products, the composition of condensate, and the treatment methods employed; thus, these elements generate intricate variability patterns. A significant number of processes in petroleum refineries consume substantial quantities of water. Therefore, refineries produce a considerable effluent containing hydrocarbons, heavy metals, and hazardous substances [4]. Organic pollutants such as phenolic compounds, chlorides, antibiotics, and others originate from companies involved in petroleum, dyestuffs, pharmaceuticals, or pesticides. These non-biodegradable pollutants have the potential to accumulate in organisms over time, resulting in cancer development. Even after a significant prohibition period, organisms still contain traces of these prohibited pollutants [5]. The study by Grmasha *et al.* [6] on the Tigris

River and its estuaries involved six months of measurement campaign for 16 PAHs; it determined the amount of these compounds present in the surface water from the oil refineries. Results showed that concentrations of the 16 PAHs in water ranged from (567.8 to 3750.7) ng/l. The highest concentrations of PAHs ranged from (49.41–81.67) %. All the PAHs in the water samples were found to be high molecular weight with (5–6) rings. Sixteen PAHs were detected in water samples taken from the Tigris River, and most of these PAHs were produced by pyrogenic sources. The toxins in oil refinery effluent adversely affect various organs in both animals and humans, including the liver, kidneys, respiratory system, lungs, and skin. Pollutants from the oil sector have been reported to raise the incidence of many cancers, including bladder, breast, colon, and prostate [7]. Microbial synthesis of nanoparticles (NPs) is an eco-friendly approach to sustainable manufacturing that employs microbiology and nanotechnology [8]. Microbes synthesize NPs through various processes, such as metal complexation, changes in solubility, extracellular precipitation, biosorption, oxidative-reductive reactions, and the absence of specific transporters and efflux pumps [9].

Bacillus and *Klebsiella* species possess iron reductase (thu) and cysteine desulfurase (suf) genes, which play a role in the biosynthesis of IONPs [10]. Iron-reducing bacteria, such as *Shewanella* spp., exhibit variable surface charge potentials depending on the composition of their cell walls. These changes, which occur under different growth conditions, have been suggested to influence the properties of nanomaterials synthesized by these bacteria [11]. The metal-reducing bacteria can couple the oxidation of various electron donors, such as lactate, pyruvate, and hydrogen to reduce different metal species, leading to the biomineralization of various metal NPs [12].

Iron oxides, comprising wustite (FeO), hematite (α-Fe_2O_3), maghemite (γ-Fe_2O_3), and magnetite (Fe_3O_4), are exceptional nanomaterials. Iron oxide nanoparticles (IONPs) exhibit superparamagnetic large surface area and biocompatibility at nanoscale, rendering them suitable for many applications. Their impact on material behavior, interaction with light, electricity, magnetism, and non-toxicity in biological systems make them promising in biomedicine and bioremediation [13]. Diverse IONPs have been extensively investigated as remediation agents in advanced oxidation processes for small organic molecules, magnetized coagulation, and as an effective adsorbent for removing pollutants from effluent [14].

IONPs act as semiconductor photocatalysts to convert pollutants into less toxic compounds and as nano-adsorbents to improve adsorption techniques to eliminate pollutants [15]. IONPs possess various characteristics, such as the ability to be modified on their surface by different substances and functional groups. This allows them to effectively remove specific pollutants through physical and chemical processes, including adsorption, reduction, precipitation, and disinfection [16]. The photodegradation of organic contaminants on the surfaces of biologically synthesized nanomaterials under sunlight exposure is an effective method for water treatment [17].

IONPs are excellent at photocatalytic degradation because they are very active, inexpensive catalysts and do not require much energy. Consequently, this technology has enormous potential for effectively removing many dyes, heavy metals, and organic pollutants from the environment [18]. To clean up water, IONP has been utilized extensively as an adsorbent (FeOOH, Fe_2O_3, and Fe_3O_4) NPs [19]. IONPs remove pyrene and benzo(a)pyrene from water with removal efficiencies (98.5 and 99) %, respectively [20]. Fe_2O_3 NPs are very effective in removing and degrading BTEX (benzene, toluene, ethylbenzene, and xylene). According to the findings, the highest BTEX removal effectiveness (90.94%) was found at pH (3.64), (167) mg/l of nanoparticle concentration, and (180) W of light intensity [21]. During the photocatalytic process, NPs transform organic pollutants into H_2O, CO_2, and reactive oxidizing species like air or oxygen [22]. The study aims to treat crude oil-contaminated water using an effective and environmentally sustainable method that employs bacteria-synthesized IONPs.

2. Materials and methods

2.1. Bacterial isolation and identification

Bacteria were Isolated from sludge samples collected from the Shuaiba refinery. One gram of sludge was transferred to a flask containing (100) ml of distilled water (D.W) and placed in a shaking incubator for an hour. After a series of dilutions of 10^{-5}, 0.1 ml was transferred from the medium to sterile nutrient agar using the spreading method, and the medium was incubated for (24) hrs at (37) °C [23]. Pure isolates were taken and cultured for purity. A pure colony was selected and stained using a Gram stain Kit. DNA was extracted using the Geneaid extraction kit, and the *16rRNA* gene was amplified using primers 27 F (AGAGTTTGATCCTGGCTCAG) and 1492R (GGTTACCTTGTTACGACTT) [24]. PCR

reactions were conducted according to the specified program in Table (1).

After sequencing the *16S rRNA* PCR product of the specified strain, a multiple sequence alignment was performed using the NCBI database as a reference.

2.2. Biosynthesize of IONPs

The bacterial isolate was activated by inoculating freshly cultured bacteria into Erlenmeyer flask containing nutrient broth. The Erlenmeyer flasks were incubated at (37) °C in a shaker at (120) rpm for (24) hrs. The bacterial culture was centrifuged for (10) min at (4,000) rpm. The supernatant was passed through a (0.45) μm sterile syringe filter. The filter supernatant was transferred to a sterilized flask to synthesize the IONPs. $FeCl_3.6H_2O$ solution (2 mM) was mixed with the supernatant of bacteria 1:1 and adjusted to pH 9, then incubated in a shaker incubator for 2 days at (37) °C. The biosynthesize of IONPs was visually checked for color changes in the supernatant. The mixture was centrifuged at (5000) rpm for (15) min to separate IONPs; then the supernatant was discarded. IONPs were washed three times with deionized D.W. and then collected and dried in an oven at (40) °C.

2.3. Characterization of IONPs

The IONPs were analyzed using a Shimadzu Dual Beam UV-1900 UV-visible spectrophotometer, scanning wavelengths from 200 to 800 nm; the absorption spectra corresponding to the surface plasmon resonance (SPR) of the IONPs were recorded. The surface functional groups and bonds in the IONPs were analyzed using a Shimadzu FT-IR spectrophotometer. The FT-IR spectra of the bacterial supernatant were obtained to identify the functional groups involved in synthesizing IONPs (ALPHA II Compact FT-IR Spectrometer - Bruker). The FE-SEM/EDX Oxford detector was employed to analyze the characteristics of the synthesized IONPs, utilizing an electron high tension of 5000 V,

a working distance of 9.1 mm, and a magnification of 60,000×, along with a quantitative compositional study of the NPs. X-ray diffraction analysis was performed using a Philips PW 1730 diffractometer to determine the crystal structure of the IONPs. The Xpert High Score Plus software was utilized for peak indexing and phase identification. Atomic Force Microscopy (AFM) was used to analyze the size, surface texture, morphology, and roughness of the IONPs. Zeta potential analysis was performed using Brookhaven Instruments to determine the surface charge of the IONPs.

2.4. Cytotoxicity of IONPs on human red blood cells

The cytotoxicity of IONPs towards human red blood cells was tested. One ml of blood was mixed with (20) ml of sterile phosphate buffer saline (PBS) to prepare blood suspension. IONPs concentrations (2,6,12, 18, and 25) mg/ml were prepared in DMSO. The assay involved the addition of (100) μl of each concentration to a test tube containing (2) ml of blood suspension. The test tube was incubated at (37)°C and observed for turbidity during a duration of (3–24) hrs. The blood suspension with (1) % NaCl solution served as a positive control, whereas the negative control was normal saline and DMSO with blood suspension. Turbidity in the blood suspension indicated a positive result and toxicity, while a nontoxic result kept the solution clear.

2.5. Evaluation of photocatalytic degradation of crude oil by IONPs

2.5.1. The effect of the concentration of IONPs on photocatalytic degradation crude oil

The photocatalytic degradation of crude oil by IONPs was evaluated by preparing different concentrations of IONPs (0.2, 0.4, 0.6, 0.8, and 1) mg/ml, which were added to an Erlenmeyer flask containing (100) ml of water and (0.5) ml of crude oil after 14 days. The experiment was conducted at room temperature under direct sunlight exposure. The degradation of crude oil was measured using a spectrofluorometer, and the degradation percentage was calculated using the following equation:

Degradation% = (A−B)/A × 100

A: Control crude oil concentration after 14 days (without IONPs).

B: Sample crude oil concentration after 14 days (with IONPs).

Table 1. PCR program for amplifying 16S rRNA.

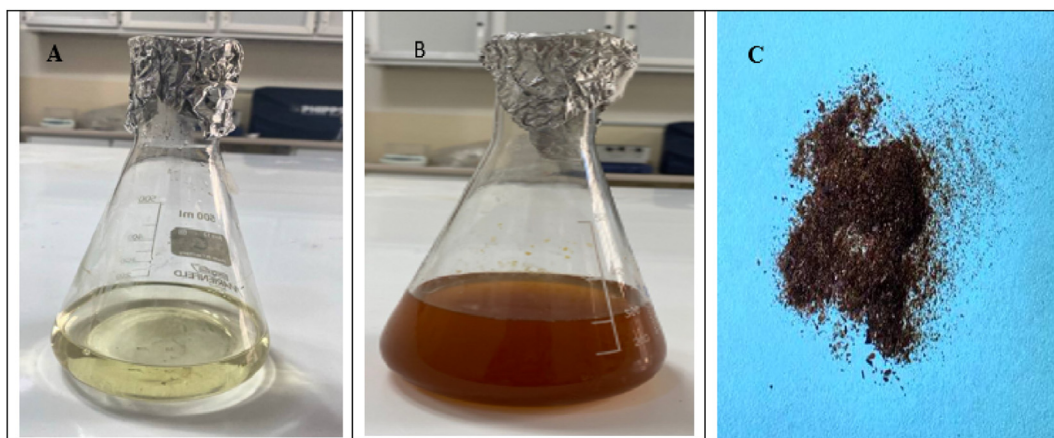| Stage	Temp	Time	Cycle	Size of product
Initial denaturation	94 °C	5 min	1	1500 bp
Denaturation	94 °C	30 sec	27	
Annealing	55 °C	35 sec		
Extension	72 °C	45 sec		
Final extension	72 °C	10 min	1	
Cooling	4 °C			

Fig. 1. Biosynthesize of Fe₂O₃ NPs (A) Supernatant of Alishewanella Jeotgali strain HAQ8 (B) mixture of supernatant and FeCl₃.6H₂O after 2 days (C) Fe₂O₃ NPs powder after drying.

2.5.2. Effect of pH on photocatalytic degradation crude oil by IONPs

The test was conducted using the IONPs concentration that achieved the highest crude oil degradation percentage. The effect of pH was evaluated at pH (5, 7, and 9). The effect of IONPs and pH on crude oil degradation after 14 days was assessed as described in the previous section.

3. Results and discussion

3.1. Bacterial isolation and identification

Molecular characterization of the *16S rRNA* gene indicated that the isolate obtained from oil refinery sludge in Basrah was identified (99.35) % with *Alishewanella jeotgali* Kctc22429 (NR_116459). *Alishewanella jeotgali* strain HAQ8 (OR885471) was registered in the gene bank database as a new strain. Most studies have used the *16S rRNA* genes to characterize bacteria [25—28]. The *16S rRNA gene*, present in nearly all bacterial species, has maintained its function over time and possesses a sufficient length of approximately 1500 bp for computational analysis. Consequently, scientists extensively use this gene for bacterial identification, taxonomy, and the elucidation of evolutionary relationships among various bacterial species [29].

3.2. Biosynthesize of IONPs

*The mixture of supernatant and FeCl₃·6H₂O solution color changed from yellow to brown over (2) days, indicating the presence of IONPs. This finding corresponds with the results of [30,31]. A green method for synthesizing metal NPs and their oxides is used as an alternative to chemical and physical techniques. It is more environmentally friendly, easily scalable, cost-effective, and does not require severe conditions such as high temperatures or toxic chemicals [32]. The extracellular method involves the reduction of metal ions, including Fe, by proteins, components of microbial cell walls, or enzymes [33]. The above components function as stabilizers and reducing agents, inhibiting the agglomeration of IONPs [34]. *Alishewanella Jeotgali* strain HAQ8 was used to synthesize IONPs at a cost of less than ten dollars, including the cost of Nutrient broth and FeCl₃·6H₂O for 5g of IONPs Fig. 1.

3.3. Characterization of IONPs

The SPR of the prepared Fe₂O₃ NPs was confirmed using UV-Vis spectrophotometry analysis. The λmax of IONPs synthesized by the *Alishewanella Jeotgali* strain HAQ8 was observed at (358) nm, Fig. 2, which falls within the reported range of (350-400) nm for the IONPs [35]. A broad band at
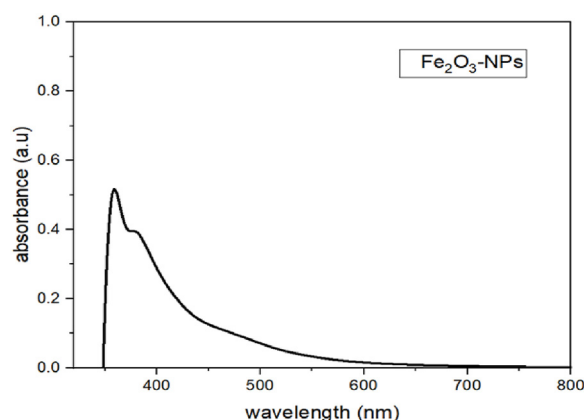

Fig. 2. The λmax of Fe₂O₃ NPs synthesized by Alishewanella jeotgali strain HAQ8 was observed at 358 nm.

---

* Special description of the title. (dispensable).

(349) nm in UV-Vis spectroscopy indicates the presence of IONPs [36]. The absorption peak of IONPs is observed at 394 nm [37]. This is due to the surface plasmon resonance of Fe_2O_3NPs. The collective oscillation of electrons in metallic NPs creates a SPR absorption band [38].

The effect of bioactive compounds in the bacterial supernatant on reducing iron ions and stabilizing IONPs was studied using Fourier Transform Infrared Spectroscopy (FTIR). The functional groups (C-H, C-C, C-H, and C-O) are present at (2911,1577,1391, and 1072) cm^{-1} in the supernatant, whereas the function groups (O-H, C-H, C-C, N-O, and C-O) are present at (3411,2924,1651, 1531.8, and 1064) cm^{-1} in IONPs, Fig. 3. The FT-IR spectra of the synthesized IONPs closely resemble those of the bacterial supernatant, suggesting that the bioactive compounds present in the supernatant serve as reducing agents for iron ions and as capping agents, contributing to the stabilization of the nanoparticles. The peak at (485) cm^{-1} matches the maghemite (Fe-O) stretching modes, proving that the prepared NPs are iron oxide Table 2. This finding is attributed to Ref. [39]. The Fe-O stretches appear in the mixture when an absorption peak is detected at (474) cm^{-1},
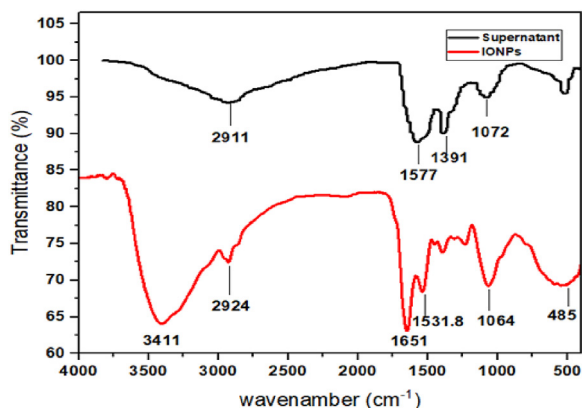
corresponding to Fe_2O_3NPs [40]. The functional groups in the molecular chains of the supernatant enhance its binding capacity [41]. The OH group's presence plays a major role in the reduction and stabilization of NPs during synthesis [42]. The functional groups responsible for reducing and capping previously mentioned IONPs are hydroxyl, alkyl, and carboxylic groups, facilitating iron salt reduction into Fe_2O_3NPs [43]. The metabolism of microorganisms produces bioactive chemicals that stop reduced iron particles from sticking together during synthesis [40].

The XRD pattern was analyzed within the range of 10° to 80° at 2θ (diffraction angle). The major diffraction peaks at 2θ (18.3°, 27.7°, 31.6°, 34.3°, 35.9°, 56.8°, 73°) correspond to the lattice planes (100, 007, 008, 113, −114, 135, −216), respectively, Fig. 4. The XRD showed the IONPs' average crystallite size was (19) nm. Furthermore, detecting numerous low-intensity peaks suggests the presence of biological molecules on the particle surfaces. The magnetic NPs made of iron oxide have an XRD pattern that matches the standard card for Fe_2O_3 (JCPDS file card number 0-076-1821) with a hexagonal phase. This result corresponds to the previous studies [44−47]. Additionally, the XRD pattern exhibited three additional peaks at 2θ = 11.7°, 23.6°, and 45.8°, which may be caused by supernatant biomolecules that cap the synthesized NPs [48]. Most peaks were sharp, indicating that the material was impure and included components that acted as capping agents. Intense Bragg reflections suggest the presence of strong X-ray scattering centers in the crystalline phase, which could be attributed to the capping agents [49]. IONPs size, morphology, surface texture, and roughness were characterized using the

Fig. 3. FT-IR spectra of (a) Alishewanella jeotgali strain HAQ8 supernatant used for synthesized Fe_2O_3 NPs (b) Fe_2O_3 NPs.

Table 2. FT-IR spectrum analysis showed the main function groups present in IONPs.

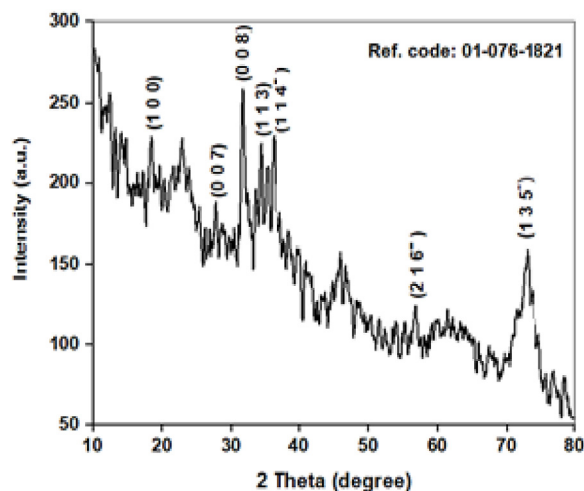| IONPs wavenumber (cm^{-1})	Appearance	Bands	Functional group
3411	Strong and broad	O−H stretching	Alcohol
2924	Medium	C−H stretching	Alkane
1651	Strong	C=C stretching	Alkene
1531.8	Strong	N-O stretching	Nitro compound
1064	Strong	C-O stretching	Primary alcohol
485	Medium	Fe-O Band	Oxide group

Fig. 4. The XRD of Fe_2O_3 NPs synthesized by Alishewanella jeotgali strain HAQ8.

AFM technique. According to AFM findings, the mean diameter of NPs was (48.8) nm, as shown in the histogram. The histogram showing most NPs was a small Fig. 5a. The three-dimensional (3D) AFM images revealed a spherical shape. The maximum height of IONPs was 18.36 nm, as shown in three-dimensional(3D) AFM images, Fig. 5b. The surface roughness parameter of IONPs is at (4.86) nm size scan. This result agrees with [50]. The spherical shape of IONPs is essential because it provides a consistent and symmetrical configuration that is beneficial for various applications. The high surface area-to-volume ratio of spherical NPs makes them more reactive and suitable for catalysis, sensing, and drug delivery and more stable and reactive [51].

In Fig. 6, SEM images of the produced IONPs showed spherical shapes with a diameter range (13.67 -85.99) nm. The size of the IONPs was between 30 nm and 60 nm [52]. The FESEM images showed the particle's spherical shape [53].

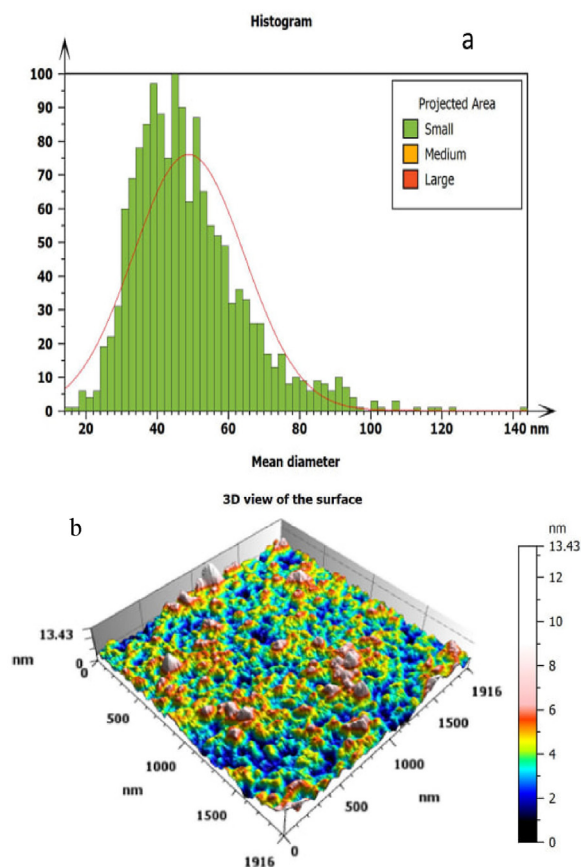The purity of synthesized IONPs was studied using EDX spectroscopy. The EDX spectra in Table 3
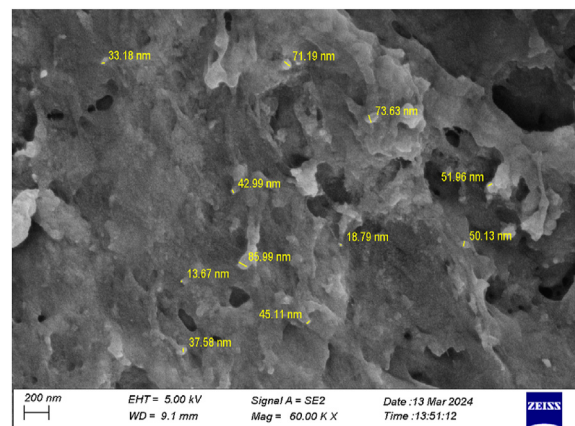

Fig. 6. The SEM shows the shape and the particle size of Fe_2O_3NPs.

Table 3. The EDX shows the percentages of chemical elements in Fe_2O_3NPs.

Element	Weight %	Weight % Sigma	Atomic %
C	50.88	0.89	62.08
O	26.59	0.57	24.35
Na	4.22	0.11	2.69
Cl	3.33	0.09	1.38
Fe	6.38	0.2	1.68
P	1.31	0.06	0.62
N	6.62	1.34	6.92
S	0.31	0.05	0.14
K	0.19	0.04	0.07
Ca	0.16	0.04	0.06
Total	100		100

showed iron peaks and other elements. The weight percentage of Fe was (6.38%), while the weight percentage of O was (26.59 %). Elements such as oxygen and carbon were identified in the supernatant sample and constitute a significant amount. Additionally, Na, S, P, Cl, K, Fe, and Ca constitute the production medium (nutrient broth) used for the growth of bacteria and the composition of salt ($FeCl_3.6H_2O$).

The most essential peaks found in this study were Fe and O, which showed the presence of IONPs and C. These may have come from the extracellular bacterial matrix in the supernatant [52]. The peaks at 6.41 keV correspond to iron's binding energies, while the oxygen peak is 0.5 keV Fig. 7. This outcome is related to Refs. [54,55].

A zeta potential analysis was conducted to determine the electrical charge on the surface of IONPs. The results showed a zeta potential value of (−43.25) mV, indicating that the NPs are stable Fig. 8. IONPs with an average zeta potential of (+41) mV were prepared from an extract of the plant Ceratonia siliqua L. that was mixed with water [56]. The extracellular technique (Proteus vulgaris ATCC-29905) was
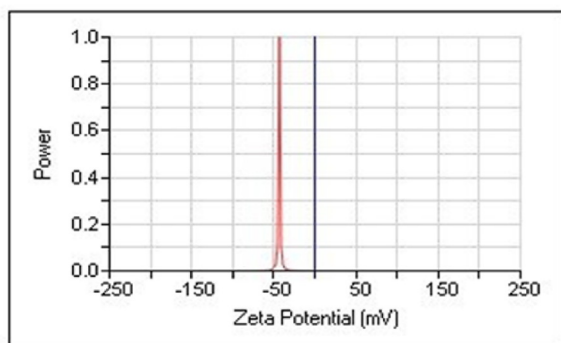

Fig. 5. (a) The Histogram and (b) 3D image (AFM) show particle distribution of Fe_2O_3NPs.
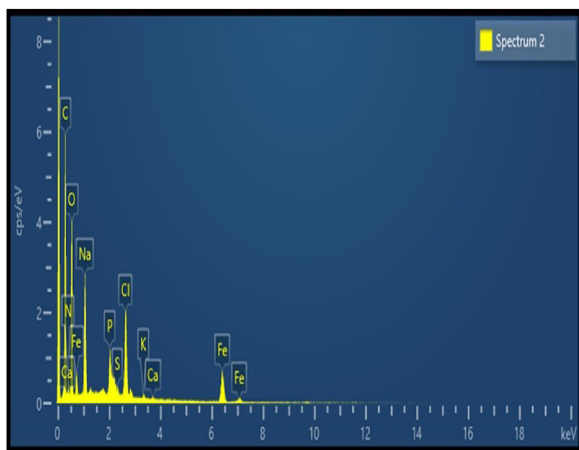
Fig. 7. The EDX shows the chemical elements in Fe_2O_3NPs.

Fig. 8. The Zeta potential analysis shows the charge of Fe_2O_3 NPs.

used to produce IONPs. The Zeta potential of IONPs was (79.5) mV, which confirms its stability [53]. The extracellular method uses genes, peptides, or proteins as reducing agents to break down iron ions into NPs with a tiny distribution spread evenly. These NPs are stable and stop IONPs from sticking together [57].

3.4. Cytotoxicity of Fe_2O_3 NPs on human red blood cells

The cytotoxicity of Fe_2O_3 NPs against human red blood cells was examined at concentrations (2, 6, 12, 18, and 25) mg/ml. The cytotoxicity results of Fe_2O_3 NPs indicated they were biocompatible with red blood cells even at the highest concentration, Fig. 9. Capping agents such as polysaccharides surrounding nanoparticles may have enhanced their blood compatibility [58]. According to the zeta potential analysis, the Fe_2O_3 NPs surface has a negative charge that repels red blood cells with the same charge. The surface charge of IONPs may induce genotoxicity and cytotoxicity. The positively charged IONPs demonstrated increased toxicity due to non-specific interactions with negatively
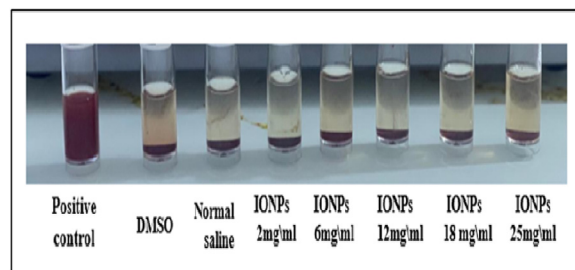

Fig. 9. The cytotoxicity of IONPs at different concentrations against human red blood cells. Evaluation of photocatalytic degradation of crude oil by IONPs.

charged cell membranes, resulting in enhanced intracellular accumulation and disruption of membrane integrity [59].

3.4.1. The effect of the concentration of IONPs on photocatalytic degradation crude oil

Five concentrations (0.2, 0.4, 0.6, 0.8, and 1) mg/l of IONPs were tested in degrading crude oil in wastewater. The results showed that the degradation percentage was (69.08, 57.93, 46.8, 34.03, and 11.90) %. The highest degradation percentage was 69.08% in the concentration of IONPs, which was 0.2 mg/l, Fig. 10. A low concentration of Fe_2O_3NPs was better than high concentrations in crude oil degradation. The result matched with previous studies [60,61]. Excessive increases in NPs concentration lead to agglomeration, markedly reducing the accessible surface area for adsorption and decreasing the number of active sites, affecting overall adsorption effectiveness [62]. The NPs' small size increases the surface area, enhancing their chemical reactivity and potential for adsorbing various contaminants onto their surfaces [63]. Using Fe_2O_3 NPs makes it easier to break down hydrocarbons without a catalyst. Another excellent thing
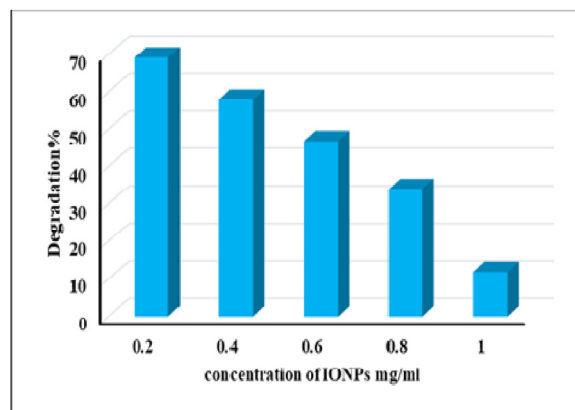

Fig. 10. The percentage of degradation of crude oil by different concentrations of Fe_2O_3NPs.

about this treatment method is that it produces no secondary pollutants. The established treatment technique may be extensively used as an economical and environmentally friendly method for managing petroleum industries. Fe_2O_3NPs have shown the capacity to disrupt the aggregation of asphaltene molecules, halting interactions between clusters and reducing oil viscosity [64]. Magnetite NP could eliminate approximately 65% of higher-chain (C23−C26) and 70% of lower-chain alkanes (C9−C22) [65]. IONPs interact with petroleum-derived contaminants in aquatic environments through adsorption, photocatalytic oxidation, and synergistic biodegradation [66]. IONPs exhibit distinctive properties, including the capacity to absorb a broad spectrum of visible light and generate highly reactive oxygen species, which can improve degradation efficiency and reduce aggregation, thereby facilitating the remediation of water contaminants [67]. The photocatalytic reaction commences. When a photon with energy (hv) equal to or surpasses the semiconductor photocatalytic NPs' band gap is absorbed. Consequently, electrons (e−) and positive holes (h+) are generated on the surface of nano photocatalysis due to the transfer of electrons via photo absorption from the valence band to the conduction band. The interactions between water and positive holes in the conduction band generate hydroxyl radicals (OH) [22].

3.4.2. Effect of pH on photocatalytic degradation crude oil by IONPs

The pH (9, 7, 5) was used with 0.2 mg/ml of IONPs for 14 days to investigate the effect on the degradation of crude oil. The results show that the best pH contributed to enhancing the degradation of crude oil by IONPs to 71.4%, which was 9, Fig. 11. Fatty acids in the aliphatic component of crude oil and those produced by the gradual oxidation of long-chain hydrocarbons react with sodium
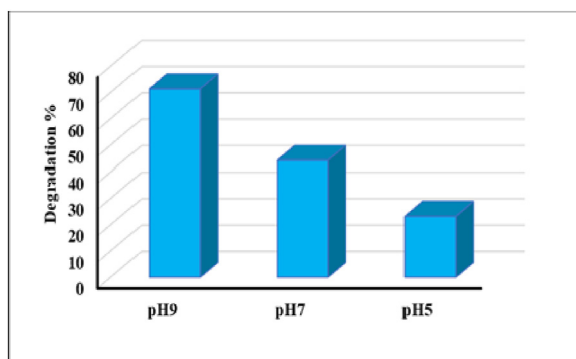
hydroxide solution [68]. Injecting alkaline substances like NaOH, which elevates the pH of aqueous solutions, effectively decreases interfacial tension values through the in-situ production of surfactants and the saponification of organic acids present in model oils [69].

In the present study, the degradation percentage of crude oil by IONPs was decreased at low pH. This behavior is attributed to the competition between protons and pollutants for active binding sites on the surface of IONPs. At lower pH, these active sites become protonated due to the excess protons, thereby diminishing the pollutant's capacity to adhere to the adsorbent [70].

4. Conclusions

Alishewanella jeotgali strain HAQ8, isolated from the sludge of an oil refinery treatment plant in Basrah government, southern Iraq, effectively synthesizes IONPs. The IONPs synthesized by the *Alishewanella jeotgali* strain HAQ8 have a diameter of less than 100 nm, a spherical shape, and a negative charge. XRD identifies IONPs as Fe_2O_3NPs. All concentrations of Fe_2O_3 NPs have no cytotoxicity against red blood cells. At 0.2 mg/ml, Fe_2O_3NPs were effective in degrading crude oil. pH 9 enhances the degradation of crude oil by Fe_2O_3NPs. Future studies aim to synthesize IONPs through cost-effective methods and utilize IONPs in bioreactors to treat polluted water.

Ethics information

None.

Conflict of interest

The authors declare that they have no competing interests.

Fig. 11. The percentage of degradation crude oil at different pH by using IONPs.

References

[1] L. Pu, Y.J. Zeng, P. Xu, F.Z. Li, M.H. Zong, J.G. Yang, W.Y. Lou, Using a novel polysaccharide BM2 produced by

Bacillus megaterium strain PL8 as an efficient bioflocculant for wastewater treatment, Int. J. Biol. Macromol. 1 (2020) 374–384, https://doi.org/10.1016/j.ijbiomac.2020.06.167.

[2] F. Akhter, S.A. Soomro, M. Ahmed, Plant and non-plant based polymeric coagulants for wastewater treatment, J. Kejuruter. 33 (2021) 175–181, https://doi.org/10.17576/jkukm-2021-33(2)-02Plant.

[3] F. Ahmad, M.M. Salem-Bekhit, F. Khan, S. Alshehri, A. Khan, M.M. Ghoneim, H.F. Wu, E.I. Taha, I. Elbagory, Unique properties of surface-functionalized nanoparticles for bio-application: functionalization mechanisms and importance in application, Nanomaterials 12 (2022) 1333, https://doi.org/10.3390/nano12081333.

[4] C.O. Akintayo, O.H. Aremu, W.N. Igboama, S.M. Nelana, O.S. Ayanda, Performance evaluation of ultra-violet light and iron oxide nanoparticles for treating synthetic petroleum wastewater: kinetics of cod removal, Materials 14 (2021) 11, https://doi.org/10.3390/ma14175012.

[5] S. Guo, H. Wang, W. Yang, H. Fida, L. You, K. Zhou, Scalable synthesis of Ca-doped α-Fe_2O_3 with abundant oxygen vacancies for enhanced degradation of organic pollutants through peroxymonosulfate activation, Appl. Catal. B Environ. 262 (2020) 118250, https://doi.org/10.1016/j.apcatb.2019.118250.

[6] S. Khan, N. Akhtar, S.U. Rehman, S. Shujah, E.S. Rha, M. Jamil, *Bacillus subtilis* synthesized iron oxide nanoparticles (Fe_3O_4 Nps) induced metabolic and Anti-Oxidative response in rice (*Oryza sativa l.*) under arsenic stress, Toxics 10 (2022) 18, https://doi.org/10.3390/toxics10100618.

[7] S. Mukherjee, C.R. Patra, Biologically synthesized metal nanoparticles: recent advancement and future perspectives in cancer theranostics, Future Sci. OA. 3 (2017) 4, https://doi.org/10.4155/fsoa-2017-0035.

[8] L. Gao, K. Fan, X. Yan, Iron oxide nanozyme: a multifunctional enzyme mimetic for biomedical applications, Theranostics 7 (2017) 3207–3227, https://doi.org/10.7150/thno.19738.

[9] R.A. Grmasha, C. Stenger-Kovács, B.A.H. Bedewy, O.J. Al-Sareji, R.A. Al-Juboori, M. Meiczinger, K.S. Hashim, Ecological and human health risk assessment of polycyclic aromatic hydrocarbons (PAH) in Tigris river near the oil refineries in Iraq, Environ. Res. 227 (2023) 115791, https://doi.org/10.1016/j.envres.2023.115791.

[10] O.B. Daramola, R.C. George, N. Torimiro, A.A. Olajide, Insights on the synthesis of iron-oxide nanoparticles and the detection of iron-reducing genes from soil microbes, Colloids Surf. C: Environ. Aspects. 2 (2024) 100025, https://doi.org/10.1016/j.colsuc.2023.100025.

[11] S. Parthasarathy, T.S. Chandra, Crystallite structure and magnetic characteristics of iron oxide nanoparticles biomineralized by *Shewanella spp.* with different surface charge potentials, J. Magn. Magn Mater. (2025) 172814, https://doi.org/10.1016/j.jmmm.2025.172814.

[12] V.D. Rajpu, T. Minkina, R.L. Kimber, V.K. Singh, S. Shende, A. Behal, S. Sushkova, S. Mandzhieva, J.R. Lloyd, Insights into the biosynthesis of nanoparticles by the genus *Shewanella*, Environ. Microbiol. 87 (2021) e01390–e10421, https://doi.org/10.1128/AEM.01390-21.

[13] P. Kumar, N. Thakur, K. Kumar, S. Kumar, A. Dutt, V.K. Thakur, C. Gutiérrez-Rodelo, P. Thakur, A. Navarrete, N. Thakur, Catalyzing innovation: exploring iron oxide nanoparticles-Origins, advancements, and future application Horizons, Coord. Chem. Rev. 507 (2024) 215750, https://doi.org/10.1016/j.ccr.2024.215750.

[14] F.I. El-Dib, D.E. Mohamed, O.A.A. El-Shamy, M.R. Mishrif, Study the adsorption properties of magnetite nanoparticles in the presence of different synthesized surfactants for heavy metal ions removal, Egypt. J. Petrol. 29 (2020) 1–7, https://doi.org/10.1016/j.ejpe.2019.08.004.

[15] W.K. Biftu, K. Ravindhranath, M. Ramamoorty, New research trends in the processing and applications of iron-based nanoparticles as adsorbents in water remediation methods, Nanotechnol. Environ. Eng. 5 (2020) 12, https://doi.org/10.1007/s41204-020-00076-y.

[16] G.N. Hlongwane, P.T. Sekoai, M. Meyyappan, K. Moothi, Simultaneous removal of pollutants from water using nanoparticles: a shift from single pollutant control to multiple pollutant control, Sci. Total Environ. 656 (2019) 808–833, https://doi.org/10.1016/j.scitotenv.2018.11.257.

[17] C. Hitam, A. Jalil, A review on an exploration of Fe_2O_3 photocatalyst towards the degradation of dyes and organic contaminants, J. Environ. Manag. 258 (2020) 110050, https://doi.org/10.1016/j.jenvman.2019.110050.

[18] T. Luo, C. Yang, X. Tian, W. Luo, Y. Nie, Y. Wang, Application of iron oxide nanomaterials for the removal of heavy metals, in: O.V. Kharissova, L.M.T. Martínez, B.I. Kharisov, eds., Handbook of Nanomaterials and Nanocomposites for Energy and Environmental Applications, Springer, Cham. 2020, p. 25, https://doi.org/10.1007/978-3-030-11155-7_76-1.

[19] S.S. Hassan, H.I. Abdel-Shafy, M.S. Mansour, Removal of pyrene and benzo (A) pyrene micropollutant from the water via adsorption by green synthesized iron oxide nanoparticles, Adv. Nat. Sci. Nanosci. Nanotechnol. 9 (2018) 015006, https://doi.org/10.1088/2043-6254/aaa6f0.

[20] A.B. Siddique, M.A. Shaheen, A. Abbas, Y. Zaman, A. Ali, M. Naeem-ul-Hassan, J. Iqbal, Photocatalytic and biological efficacy of Carissa macrocarpa fruit extract-mediated one-pot synthesized ternary metal oxide dual S-scheme heterojunction, J. Environ. Chem. Eng. 12 (2024) 112725, https://doi.org/10.1016/j.jece.2024.112725.

[21] Z. Sheikholeslami, D.Y. Kebria, F. Qaderi, Application of γ-Fe_2O_3 nanoparticles for pollution removal from water with visible light, J. Mol. Liq. 299 (2020) 112118, https://doi.org/10.1016/j.molliq.2019.112118.

[22] A. Bouafia, S. Meneceur, S. Chami, S.E. Laouini, H. Daoudi, S. Legmairi, H.A.M. Mohammed, N. Aoun, F. Menaa, Removal of hydrocarbons and heavy metals from petroleum water by modern green nanotechnology methods, Sci. Rep. 13 (2023) 14, https://doi.org/10.1038/s41598-023-32938-1.

[23] S.G. Mulamattathil, C. Bezuidenhout, M. Mbewe, C.N. Ateba, Isolation of environmental bacteria from surface and drinking water in Mafikeng, South Africa, and characterization using their antibiotic resistance profiles, J. Pathog. 2014 (2014) 371208, https://doi.org/10.1155/2014/371208.

[24] T. Miyoshi, T. Iwatsuki, T. Naganuma, Phylogenetic characterization of 16S rRNA gene clones from deep-groundwater microorganisms that pass through 0.2-micrometer-pore-size filters, Appl. Environ. Microbiol. 71 (2005) 1084–1088, https://doi.org/10.1128/AEM.71.2.1084-1088.2005.

[25] E.M. Aboud, A. Burghal, A.H. Laftah, Genetic identification of hydrocarbons degrading bacteria isolated from oily sludge? And petroleum-contaminated soil in Basrah City, Iraq, Biodiversitas 22 (2021) 1934–1939, https://doi.org/10.13057/biodiv/d220441.

[26] S.A. Gmais, A.A. Burghal, Molecular identification of oil-utilizing bacteria isolated from oil-contaminated soils in Basrah City, Appl. Biochem. Microbiol. 58 (2022) 182–188, https://doi.org/10.5281/zenodo.7485637.

[27] M.H.H. Al-Zaidi, W.H. Al-Tamimi, A. Saleh, Molecular determination of the microbial diversity associated with vaginitis and testing their sensitivity to selected antimicrobials, Biodiversitas 24 (2023) 4253–4261, https://doi.org/10.13057/biodiv/d240806.

[28] H.Q. Al-assay, W.H. Al-Tamimi, A.F. Almansoory, Extracellular synthesis of iron oxide NPs by using several bacteria genera isolated from oil contaminated sites in Basrah Governorate, Egypt, J. Aquat. Biol. Fish. 28 (2024) 1895–1914, https://doi.org/10.21608/ejabf.2024.375219.

[29] M. Palma-Jiménez, M. Blanco-Meneses, J. Vega-Baudrit, Study of microorganisms associated with the chemical compounds in tropical soil, Int. J.Plant & Soil Sci. 21 (2018) 13, https://doi.org/10.9734/IJPSS/2018/39052.

[30] P. Periyathambi, W.S. Vedakumari, S. Bojja, S.B. Kumar, T.P. Sastry, Green biosynthesis and characterization of fibrin functionalized iron oxide nanoparticles with mri sensitivity and increased cellular internalization, Mater.

Chem. Phys. 148 (2014) 1212−1220, https://doi.org/10.1016/j.matchemphys.2014.09.050.

[31] N.A. Zakariya, W.H.W. Jusof, S. Majeed, Green approach for iron oxide nanoparticles synthesis: application in antimicrobial and Anticancer-An updated review, Karbala Int.J.Mod.Sci. 8 (2022) 421−437, https://doi.org/10.33640/2405-609X.3256.

[32] S.S. Salem, A. Fouda, Green synthesis of metallic nanoparticles and their prospective biotechnological applications: an overview, Biol. Trace Elem. Res. 199 (2021) 344−370, https://doi.org/10.1007/s12011-020-02138-3.

[33] M. Fatemi, N. Mollania, M. Momeni-Moghaddam, F. Sadeghifar, Extracellular biosynthesis of magnetic iron oxide nanoparticles by bacillus cereus strain Hmh1: characterization and in vitro cytotoxicity analysis on Mcf-7 and 3t3 cell lines, J. Biotechnol. 270 (2018) 11, https://doi.org/10.1016/j.jbiotec.2018.01.021.

[34] D. Lahiri, M. Nag, H.I. Sheikh, T. Sarkar, H.A. Edinur, S. Pati, R.R. Ray, Microbiologically synthesized nanoparticles and their role in silencing the biofilm signaling Cascade, Front. Microbiol. 12 (2021) 19, https://doi.org/10.3389/fmicb.2021.636588.

[35] V.V. Makarov, S.S. Makarova, A.J. Love, O.V. Sinitsyna, A.O. Dudnik, I.V. Yaminsky, M.E. Taliansky, N.O. Kalinina, Biosynthesis of stable iron oxide nanoparticles in aqueous extracts of Hordeum vulgare and Rumex acetosa plants, Langmuir 30 (2014) 5982−5988, https://doi.org/10.1021/la5011924.

[36] M.T. Yassin, F.O. Al-Otibi, A.A. Al−Askar, Green synthesis, characterization, and antimicrobial activity of iron oxide nanoparticles with tigecycline against multidrug-resistant bacterial strains, J. King Saud Univ. Sci. 36 (2024) 9, https://doi.org/10.1016/j.jksus.2024.103131.

[37] I. Kumar, R. Nayak, L.B. Chaudhary, V.N. Pandey, S.K. Mishra, N.K. Singh, A. Srivastava, S. Prasad, R.M. Naik, Fabrication of α-Fe$_2$O$_3$ nanostructures: synthesis, characterization, and their promising application in the treatment of carcinoma A549 lung cancer cells, ACS Omega 7 (2022) 21882−21890, https://doi.org/10.1021/acsomega.2c02083.

[38] H.G.A. Alshami, W.H. Al-Tamimi, R.R. Hateet, Screening for extracellular synthesis of silver nanoparticles by bacteria isolated from Al-Halfaya oil field reservoirs in Missan Province, Iraq, Biodiversitas 23 (2022) 3462−3470, https://doi.org/10.13057/biodiv/d230720.

[39] V.K. Yadav, D. Ali, S.H. Khan, G. Gnanamoorthy, N. Choudhary, K.K. Yadav, V.N. Thai, S.A. Hussain, S. Manhrdas, Synthesis and characterization of amorphous iron oxide nanoparticles by the sonochemical method and their application for the remediation of heavy metals from wastewater, Nanomaterials 10 (2020) 17, https://doi.org/10.3390/nano10081551.

[40] N. Sidkey, Biosynthesis, characterization and antimicrobial activity of iron oxide nanoparticles synthesized by fungi, Al-Azhar J. Pharm.Sci. 62 (2020) 164−179, https://doi.org/10.21608/ajps.2020.118382.

[41] Y. Xiong, Y. Wang, Y. Yu, Q. Li, H. Wang, R. Chen, N. He, Production and characterization of A novel bioflocculant from Bacillus licheniformis, Appl. Environ. Microbiol. 76 (2010) 2778−2782, https://doi.org/10.1128/AEM.02558-09.

[42] Y. Mata, E. Torres, M. Blazquez, A. Ballester, F. González, J. Munoz, Gold (iii) biosorption and bioreduction with the brown alga Fucus vesiculosus, J. Hazard Mater. 166 (2009) 612−618, https://doi.org/10.1016/j.jhazmat.2008.11.064.

[43] P.A. Sundaram, R. Augustine, M. Kannan, Extracellular biosynthesis of iron oxide nanoparticles by Bacillus subtilis strains isolated from rhizosphere soil, Biotechnol. Bioproc. Eng. 17 (2012) 835−840, https://doi.org/10.1007/s12257-011-0582-9.

[44] M.P. Desai, K.D. Pawar, Immobilization of cellulase on iron tolerant Pseudomonas stutzeri biosynthesized photocatalytically active magnetic nanoparticles for increased thermal stability, Mater. Sci. Eng. C 106 (2020) 110169, https://doi.org/10.1016/j.msec.2019.110169.

[45] W.J. Aziz, M.A. Abid, D.A. Kadhim, M.K. Mejbel, Synthesis of iron oxide (β-Fe$_2$O$_3$) nanoparticles from Iraqi grapes extract and its biomedical application, IOP Conf. Ser. Mater. Sci. Eng. 881 (2020) 012099, https://doi.org/10.1088/1757-899X/881/1/012099.

[46] P. Barik, N. Saharan, K.K. Krishnani, H.K. Vardia, R. Sharma, M.A. Malik, Bacteria-mediated synthesis of iron oxide nanoparticles and their efficiency in ammonia removal from fish culture tanks, Indian J. Anim. Res. 57 (2023) 1397−1406, https://doi.org/10.18805/IJAR.B-5090.

[47] R. Wahab, F. Khan, A.A. Al-Khedhairy, Hematite iron oxide nanoparticles: apoptosis of myoblast cancer cells and their arithmetical assessment, RSC Adv. 8 (2018) 24750−24759, https://doi.org/10.1039/C8RA02613K.

[48] R. Shanmugam, M. Tharani, S.S. Abullais, S.R. Patil, M.I. Karobarii, Black seed assisted synthesis, characterization, free radical scavenging, antimicrobial and anti-inflammatory activity of iron oxide nanoparticles, BMC Complement.Med.Ther. 24 (2024) 13, https://doi.org/10.1186/s12906-024-04552-9.

[49] E. Wetterskog, M. Agthe, A. Mayence, J. Grins, D. Wang, S. Rana, A. Ahniyaz, G. Salazar-Alvarez, L. Bergström, Precise control over the shape and size of iron oxide nanocrystals suitable for assembly into ordered particle arrays, Sci. Technol. Adv. Mater. 15 (2014) 055010, https://doi.org/10.1088/1468-6996/15/5/055010.

[50] P.J. Jacob, M.J. Masarudin, M.Z. Hussein, R.A. Rahim, Facile aerobic construction of iron-based ferromagnetic nanostructures by A novel microbial nano factory isolated from tropical freshwater wetlands, Microb. Cell Fact. 16 (2017) 14, https://doi.org/10.1186/s12934-017-0789-3.

[51] A.H. Mondal, D. Yadav, S. Mitra, K. Mukhopadhyay, Biosynthesis of silver nanoparticles using culture supernatant of Shewanella sp. ARY1 and their antibacterial activity, Int. J. Nanomed. 15 (2020) 8295−8310.

[52] H. Singh, J. Du, P. Singh, T.H. Yi, Extracellular synthesis of silver nanoparticles by Pseudomonas sp. THG-LS1.4 and their antimicrobial application, J. Pharm. Anal. 8 (2018) 258−264, https://doi.org/10.1016/j.jpha.2018.04.004.

[53] S. Majeed, M. Danish, M.N.M. Ibrahim, S.H. Sekeri, M.T. Ansari, A. Nanda, G. Ahmad, Bacteria mediated synthesis of iron oxide nanoparticles and their antibacterial, antioxidant, and cytocompatibility properties, J.Clust. Sci. 32 (2021) 1083−1094, https://doi.org/10.1007/s10876-020-01876-7.

[54] A.B. Taha, M.S. Essa, B.T. Chiad, Spectroscopic study of iron oxide nanoparticles synthesized via hydrothermal method, Chem Methodol 6 (2022) 977−984, https://doi.org/10.22034/CHEMM.2022.355199.1590.

[55] S. Saqib, M.F.H. Munis, W. Zaman, F. Ullah, S. Shah, A. Ayaz, M. Farooq, S. Bahadur, Synthesis, characterization, and use of iron oxide nanoparticles for antibacterial activity, Microsc. Res. Tech. 82 (2019) 415−420, https://doi.org/10.1002/jemt.23182.

[56] D. Aksu Demirezen, Ş. Yõlmaz, D. Demirezen Yõlmaz, Y.Ş. Yõldõz, Green synthesis of iron oxide nanoparticles using Ceratonia siliqua L. aqueous extract: improvement of colloidal stability by optimizing synthesis parameters, and evaluation of antibacterial activity against gram-positive and gram-negative bacteria, Int. J. Mater. Res. 113 (2022) 849−861, https://doi.org/10.1515/ijmr-2022-0037.

[57] P. Singh, Y. Kim, D. Zhang, D. Yang, Biological synthesis of nanoparticles from plants and microorganisms, Trends Biotechnol. 34 (2016) 588−599, https://doi.org/10.1016/j.tibtech.2016.02.006.

[58] N.G. Dlamini, A.K. Basson, R.V. Pullabhotla, Wastewater treatment by A polymeric bioflocculant and iron nanoparticles synthesized from A bioflocculant, Polym 12 (2020) 1618, https://doi.org/10.3390/polym12071618.

[59] B. Muthukumar, R. Duraimurugan, P. Parthipan, R. Rajamohan, R. Rajagopal, J. Narenkumar, A. Rajasekar, T. Malik, Synthesis and characterization of iron oxide

nanoparticles from *Lawsonia inermis* and its effect on the biodegradation of crude oil hydrocarbon, Sci. Rep. 14 (2024) 11335, https://doi.org/10.1038/s41598-024-61760-6.

[60] O.M. Kalfa, Ö. Yalçõnkaya, A.R. Türker, Synthesis of nano B_2O_3/TiO_2 composite material as A new solid phase extractor and its application to preconcentration and separation of cadmium, J. Hazard Mater. 166 (2009) 455–461, https://doi.org/10.1016/j.jhazmat.2008.11.112.

[61] Y. Liu, H. Zheng, Y. Sun, J. Ren, X. Zheng, Q. Sun, W. Ding, Synthesis of novel chitosan-based flocculants with amphiphilic structure and its application in sludge dewatering: role of hydrophobic groups, J. Clean. Prod. 249 (2020) 119350, https://doi.org/10.1016/j.jclepro.2019.119350. .

[62] M.A. Siddiqui, M. A, R. Wahab, Saquib, Q. Ahmad, J.N.N. Farshori, E.S. Al-Sheddi, A.A. Al-Khedhairy, Iron oxide nanoparticles induced cytotoxicity, oxidative stress, cell cycle arrest, and DNA damage in human umbilical vein endothelial cells, J. Trace Elem. Med. Biol. 80 (2023) 127302, https://doi.org/10.1016/j.jtemb.2023.127302.

[63] S.S. Ehmedan, M.K. Ibrahim, A.M. Azzam, H.A. Hamedo, A. M, Acceleration the bacterial biodegradation of crude oil pollution using Fe_2O_3 and ZnO nanoparticles, environmental nanotechnology, Monit. Manag. 16 (2021) 100613, https://doi.org/10.1016/j.enmm.2021.100613.

[64] A. Alabresm, Y.P. Chen, A.W. Decho, J. Lead, A novel method for the synergistic remediation of oil-water mixtures using nanoparticles and oil-degrading bacteria, Sci. Total Environ. 630 (2018) 1292–1297, https://doi.org/10.1016/j.scitotenv.2018.02.277.

[65] S. Yao, S. Ouyang, Q. Zhou, Z. Tao, Y. Chen, T. Zheng, Environmental remediation and sustainable design of iron oxide nanoparticles for removing petroleum-derived pollutants from water: a critical review, Environ. Res. 263 (2024) 120009, https://doi.org/10.1016/j.envres.2024.120009.

[66] A.A. Adesibikan, S.S. Emmanuel, S.A. Nafiu, M.J. Tachia, K.O. Iwuozor, E.C. Emenike, A.G. Adeniyi, A review on sustainable photocatalytic degradation of agro-organochlorine and organophosphorus water pollutants using biogenic iron and iron oxide-based nanoarchitecture materials, Desalination Water Treat. 320 (2024) 100591, https://doi.org/10.1016/j.dwt.2024.100591.

[67] M.A. Tahoon, S.M. Siddeeg, N. Salem Alsaiari, W. Mnif, F. Ben Rebah, Effective heavy metals removal from water using nanomaterials: a review, Processes 8 (2020) 645, https://doi.org/10.3390/pr8060645.

[68] M. Li, M. Lin, Z. Wu, A.A. Christy, The influence of NaOH on the stability of paraffinic crude oil emulsion, Fuel 84 (2005) 183–187, https://doi.org/10.1016/j.fuel.2004.09.001.

[69] M. Behrang, S. Hosseini, N. Akhlaghi, Effect of pH on interfacial tension reduction of oil (heavy acidic crude oil, resinous and asphaltenic synthetic Oil)/Low salinity solution prepared by chloride-based salts, J. Pet. Sci. Eng. 205 (2021) 108840, https://doi.org/10.1016/j.petrol.2021.108840.

[70] Y. Wang, X. Ma, Y. Li, X. Li, L. Yang, L. Ji, Y. He, Preparation of a novel chelating resin containing amidoxime–guanidine group and its recovery properties for silver ions in aqueous solution, Chem. Eng. J. 209 (2012) 394–400, https://doi.org/10.1016/j.cej.2012.07.143.